FATIGUE PERFORMANCE AND EIDS DISTRIBUTIONS OF WROUGHT AND POWDER-BED ADDITIVELY-MANUFACTURED Ti-6Al-4V

Matthew E. Krug[1,2], Sushant K. Jha[3], Patrick J. Golden[2], Reji John[2]

[1]matthew.krug.3@us.af.mil
[2]Air Force Research Laboratory, Materials and Manufacturing Directorate, Wright-Patterson AFB, OH, USA
[3]University of Dayton Research Institute, Dayton, OH, USA

Abstract: Powder-bed fusion additive manufacturing (PBF AM) of metals has reached an intermediate stage of technological maturity. Parts manufactured by PBF AM are considered by OEMs and end-users for a growing set of applications. To date, however, few of those applications have been fracture critical components due to uncertainties inherent in durability and damage tolerance certification of AM metals. Certification considerations specific to AM include fabrication system-to-system variability, frequent hardware and build-parameter-set updates, and non-destructive defect inspections of complex geometries to name only a few.

The US Air Force relies upon the Equivalent Initial Damage Size (EIDS) distribution to characterize the quality of an aircraft structure upon manufacture, inspection or repair. Although decades of experience with this approach inform certification of structural components produced by conventional fabrication modes (cast and wrought parts), there is little available published EIDS data for PBF AM metals. In this work we report on preliminary EIDS distribution data for PBF AM Ti-6Al-4V. EIDS distributions are in development for several hundred fatigue samples across which fabrication modality (laser- vs. electron-beam energy source), orientation, surface condition, heat treatment, and other variables are modified. The results are interpreted in a certification context by comparison with data developed in parallel for mill-annealed Ti-6Al-4V plate forgings.

Keywords: Additive manufacturing, Ti-6Al-4V, fatigue, EIDS, Durability and Damage Tolerance

INTRODUCTION

In recent years, aircraft equipment manufacturers and operators in the commercial and defense sectors have been giving increasing consideration to structural parts fabricated using additive manufacturing (AM) of metals, including powder-bed fusion AM (PBF AM). To date, however, few of those applications have been critical structural components due to uncertainties inherent in durability and

damage tolerance (DADT) certification of AM metals. Parts made by conventional fabrication routes (forging, rolling, extrusion, etc.) often benefit from conditions favorable to qualification and certification, including: simple source material, geometries amenable to non-destructive evaluation, high material quality due to thermal-mechanical processing and, most importantly, decades of qualification and certification experience. By comparison, qualification and certification procedures for metal AM parts are relatively immature. Those procedures are made more complicated by AM-specific concerns including fabrication system-to-system variability, frequent updates to hardware and build-parameter-sets, complex difficult-to-inspect geometries, and defect-rich surfaces, among other complications.

As described in MIL-STD-1530D [1], the United States Air Force (USAF) Aircraft Structural Integrity Program defines requirements necessary to consider when producing new or modified designs for aircraft structures, including their materials of manufacture. Structural components whose failure "*could… cause loss of aircraft or cause severe injury or death…,*" are termed Fracture Critical (FC); other structural components are either Durability Critical (DC) if they are judged to require additional controls, or otherwise are Normal Controls (NC) [1]. Structures Bulletin EZ-SB-19-01, which establishes requirements for DADT certification of structural components made by metal AM, recommends gaining certification experience with parts of escalating criticality beginning with NC parts before advancing to FC and DC parts [2]. The imposed DADT certification requirements on quality are similarly commensurate with part criticality. The Equivalent Initial Damage Size (EIDS) distribution is an important analytical concept for aircraft DADT analyses used by the USAF [1]. The damage size chosen for DADT analysis is based on the distribution of EIDS values calculated using the 90th percentile durability load spectrum. From this distribution an EIDS value is selected depending on part criticality and on the analysis type. The value is selected according to a prescribed probability of exceedance, but may not be less than a minimum limiting value, as shown in Table 1. Because even NC parts require completion of a durability crack growth analysis that is associated with an EIDS distribution, any effort to field structural metal AM parts in a USAF aircraft must furnish EIDS data sufficient to represent the part quality.

This manuscript describes an effort to provide to the USAF EIDS data developed for PBF AM Ti-6Al-4V. The scope of this work is limited, as it includes only a single alloy, ambient temperature testing, and round-bar lab specimens. Nevertheless, a number of important fabrication variables are explored, and the test plan includes a relatively large number of specimens to facilitate the development of data distributions rather than simply mean values. Variations in fatigue lives and in resultant EIDS values are discussed in terms of the processing history by specimen class, and where possible are linked to physical defects observed to initiate fatigue cracks. The results below add to a limited number of earlier studies which consider fatigue crack growth (FCG) data in AM metals, interpreted through the EIDS implications and discussed in a military DADT and airworthiness context [3,4].

Table 1: Damage sizes for DADT crack growth analyses [2]

Part Criticality	Durability requirement		Damage Tolerance requirement	
	P_{exceed}	$EIDS_{min}$ [mm]	P_{exceed}	$EIDS_{min}$ [mm]
NC	$1x10^{-1}$	0.25	–	–
FC or DC	$1x10^{-3}$	0.25	$1x10^{-7}$	1.3

MATERIALS AND EXPERIMENTAL PROCEDURE

The material used in this study was Ti-6Al-4V (Ti-6-4), an α+β titanium alloy that has found significant use in aerospace applications in conventionally-manufactured forms. Plasma-atomized Ti-6-4 Grade 5 powder for laser powder bed fusion (LPBF, 15-53μm) and electron-beam melting (EBM, 53-106μm) processes was supplied by AP&C, a GE Additive Company. The powder for both processes was produced from the same parent lot. The chemical composition met the ASTM F2924 specification for powder bed fusion Ti-6-4 [5]. Powder samples as well as consolidated metal samples were characterized periodically over multiple builds to confirm that the composition and particle size remained consistent for up to 17 powder reuses, the maximum reuse number in this effort.

An EOS M290 direct metal laser melting (DMLM) machine was used to produce LPBF samples. Several build layouts were used to fabricate machined-surface fatigue and as-built surface fatigue specimens. The standard layout used to manufacture predominantly machined surface fatigue specimens is shown in Fig. 1(a). This layout also included tensile test specimens and fatigue crack growth rate (FCGR) specimens. As shown in the figure, for fatigue and tensile specimens, hexagonal cross section blanks were printed in the vertical (Z) orientation (fatigue and tensile) and in the horizontal (X) orientation (fatigue only). Following post-processing heat treatment, the blanks were machined into cylindrical gauge section fatigue and tensile specimens. For FCGR specimens, rectangular blanks were printed, heat treated, and machined into a compact-tension (C(T)) specimen geometry.

A second build layout was necessary to supply the total number of required as-built surface specimens, as indicated by Fig. 1(b). Due to a slender gauge section transitioning to grip ends with larger diameter, these specimens require a support structure to mitigate any lateral force on the specimen by the recoater blade that may cause bending. In addition to as-built surface fatigue specimens, this layout also contained witness tensile specimen blanks and FCGR specimen blanks.

EBM specimens were printed using an Arcam Q10+ machine. The build layout for samples manufactured by the EBM process is shown in Fig. 1(c). Cylindrical and rectangular blanks were printed in this case and later machined into fatigue, tensile, and, FCGR specimens.

The LPBF samples were subjected to a post-process heat treatment before removal from the build plate (Table 2). The heat treatment included a combined solutionization and stress relief treatment in the α+β phase field. Microstructural analysis after the post-process heat treatment showed a Widmanstätten structure featuring alpha laths, which is typical of AM Ti-6-4. Representative samples were also characterized for porosity using metallographic analysis as well as X-ray CT. Pore volumetric number density was estimated to be approximately 1 mm^{-3}. The maximum pore equivalent diameter based on cross-sectional metallography measurements of approximately 800 pores was 77 μm.

During EBM fabrication, due to the high background temperatures generated, a stress relief heat treatment is not generally required for Ti-6-4 samples (Table 2). In this case, sample blanks were removed from the build plate and post-processed using a hot-isostatic pressure (HIP) treatment. HIP is considered necessary for EBM Ti-6-4 due to the existence of a higher degree of porosity in the as-built material than is typically present in LPBF Ti-6-4. HIP treatment reduces the size of pores, and in some cases can heal them. The temperature for HIP treatment was kept the same as the heat treatment temperature used for LPBF samples.

Tensile test sample blanks were printed on each build in order to track the tensile properties of the material across builds. The blanks were machined into round bar tensile test samples in accordance with ASTM E-8-21 [6]. Tensile tests were conducted under strain control at a strain rate of about 8.3E-5 m/m/sec.

Inputs for EIDS calculations included the stress - life (S-N) fatigue results and FCGR behavior. S-N fatigue tests were conducted in both machined-surface as well as as-printed-surface condition. Machined surface tests used round bar specimens that were machined from hexagonal sample blanks. For

specimens with an as-printed surface condition, round bar specimens were directly printed in a vertical (Z) orientation. These tests were conducted in accordance with ASTM E466-15 [7] using a MTS servo-hydraulic test system equipped with a digital controller. The tests were run in load control at room temperature. The stress ratio, R, was 0.1 and the frequency was 20 Hz. The tests were either run until failure or the designated run-out cycle count of 10^7 cycles. To determine the crack initiation mechanism, fracture surfaces of failed specimens were characterized using an FEI Quanta scanning electron microscope with a field emission gun emitter operating at 15kV accelerating voltage through a 30µm aperture.

FCGR tests were conducted using C(T) specimens that were machined from rectangular sample blanks. FCGR sample blanks were included in the layout for each build to check for consistency of FCGR behavior across builds. The orientations of C(T) specimens were X-Z and Z-X (loading direction - crack propagation direction). FCGR tests were conducted using a MTS servo-hydraulic test system in accordance with ASTM E647-15 [8]. Tests were run at room temperature at a load ratio of 0.1 and a frequency of 20 Hz. The test procedure included a standard pre-cracking step followed by either a decreasing ΔK test or an increasing ΔK test. The compliance method was used for crack length measurement throughout the test. The test frame was also equipped with optical microscopes to record optical crack length readings at specified intervals. In addition, a heat tinting method was used to mark the fracture surface at the end of the pre-crack step as well as just before fracture. Crack length measurements on fracture surfaces were used to apply a correction to compliance-based data. The FCGR raw data was analyzed using the Δa-increment method as given in [9].

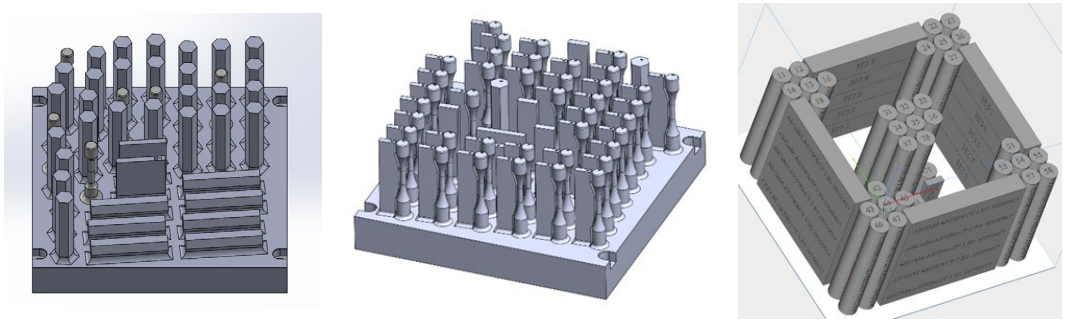

(a) (b) (c)

Fig. 1: Specimen build layouts for (a) LPBF standard layout (b) LPBF layout for as-built surface specimens and (c) EBM layout.

Table 2: Material processing variables for fatigue testing

Fabrication process / AM Platform	Material source program	Heat treatment	Surface condition	Orientation[4,5]
LPBF / EOS M290	Current	SR[1]	LSG	Z / vertical[4]
LPBF / EOS M290	Current	SR[1]	as-built	Z / vertical[4]
LPBF / EOS M290	Current	SR[1]	LSG	X / horizontal[4]
EBM / Arcam Q10+	Current	HIP[2]	LSG	Z / vertical[4]
Plate forging / –	Current	MA[3]	LSG	long.[5]
Plate forging / –	Archival	MA[3]	LSG	long.[5]

1. Combined stress-relief and solution heat treatment in vacuum
2. Hot isostatically pressed
3. Solution heat treat 932±14 °C / 1h + mill-anneal 704±14 °C / 2h
4. Z and X designate orientations parallel to build direction and to the build plane, respectively.
5. Long. designates parallel to the longitudinal direction of material flow during plate forging

RESULTS AND ANALYSIS

A summary of tensile results for LPBF specimens is given in Table 3. As shown, the mean yield strength and ultimate tensile strength, based on four tests, were 920 MPa and 1006 MPa, respectively. The mean elongation to failure was 19 %. These tensile properties meet the ASTM F2924-14 specification (powder bed fusion Ti-6Al-4V) data, which is also included in the table for comparison [5].

Table 3: Summary of tensile results on LPBF AM Ti-6Al-4V

Data source	Powder, Heat treat condition, and Build orientation		Yield strength (MPa) Mean	UTS (MPa) Mean	Elongation (%) Mean	Number of data points
ASTM F2924-14	Class A-D, minimum	XY	825	895	10	---
		Z	825	895	10	---
Current study (LPBF)	AP&C Ti-6Al-4V, Stress relief	Z	920	1006	19	4

The conditions of fatigue specimen gage section surfaces are shown in Fig. 2. The low-stress grinding procedure applied to the machined specimen gage section surfaces resulted in a longitudinal surface roughness, Ra, of approximately 0.32±0.04 µm (mean±standard deviation). All circumferential machining marks were removed during final polishing. The as-built gage sections are covered in a high density of partly-bonded powder particles, which necessitated use of cross-sectional metallography and digital analysis for surface roughness measurement. From four longitudinal traces measuring approximately 15mm in length taken from each of four samples (~240mm total) the average surface roughness of as-built samples is characterized by Ra of 16±3µm and Rv of 52±10µm.

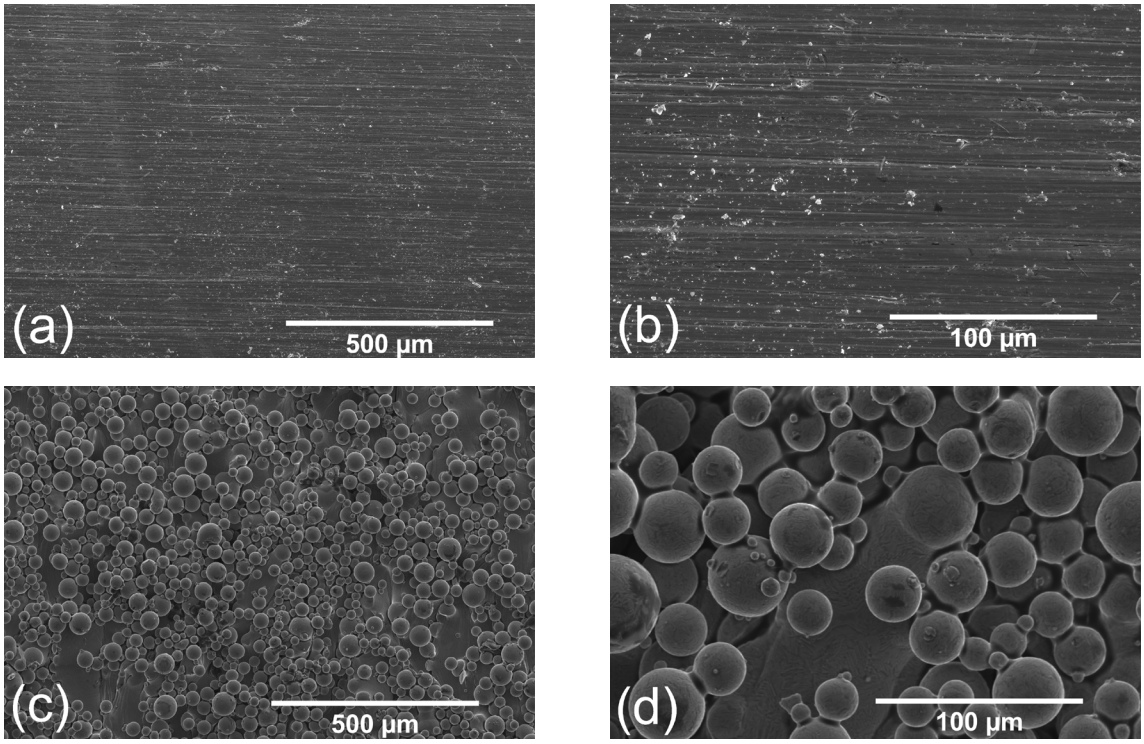

Fig. 2: Machined (a, b) and as-built (c, d) fatigue specimen gage section surfaces. For all images, the build direction and the loading direction are approximately parallel to the horizontal direction in the images.

Fatigue testing results are divided into two plots for clarity as presented in Fig. 3 (a) and (b). Archival fatigue data from an extensive, previously unpublished test series of Ti-6Al-4V forged plate (series label: wrought-archival) is also shown for comparison. The source of these Ti-6Al-4V forgings is described in [10]. Where points are indicated to be non-valid, it is always because the fatigue fracture is located outside of the uniform gage section. A large fraction (58%) of LPBF as-built specimen tests had non-valid results due to the large number of competing potential initiation sites resulting from rough surfaces, which led to frequent initiation in the transition from the gage section to the grip. Non-valid data are retained in the plot (bright red markers) because they appear to be in-family with the valid test results. The main feature of the plot is the clear classification of fatigue response into two groups. Machined specimens (label includes 'LSG'), which include both AM and wrought specimens, are higher-performing with runout maximum cycle stresses typically in the range 540-650 MPa; as-built LPBF specimens with significantly rougher surfaces are lower-performing with runout maximum cycle stresses in the range 310-330 MPa. In other words, the roughness of as-built surfaces allow a part which retains only about half of the inherent material capability. This is true even for the vertical as-built surfaces reported here, which in general have a higher quality than more challenging surfaces such as overhangs or unsupported roofs. Within the groups of machined samples, the fatigue life distributions of AM specimens tends to be wider than those of wrought specimens, with the shortest AM fatigue lives being smaller than wrought, and the longest AM fatigue lives also being larger than those of the wrought

specimens. Among the two wrought series, the current and archival forged-plate specimens perform similarly up to maximum cycle stresses of 750MPa, above which no testing was performed in the archival testing.

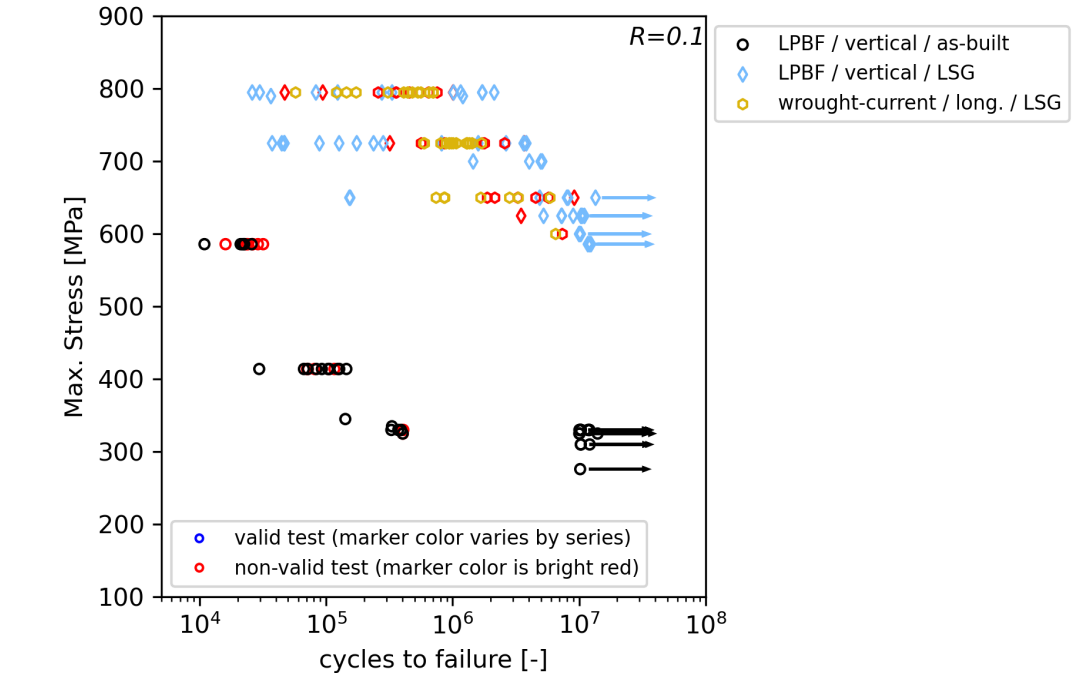

(a)

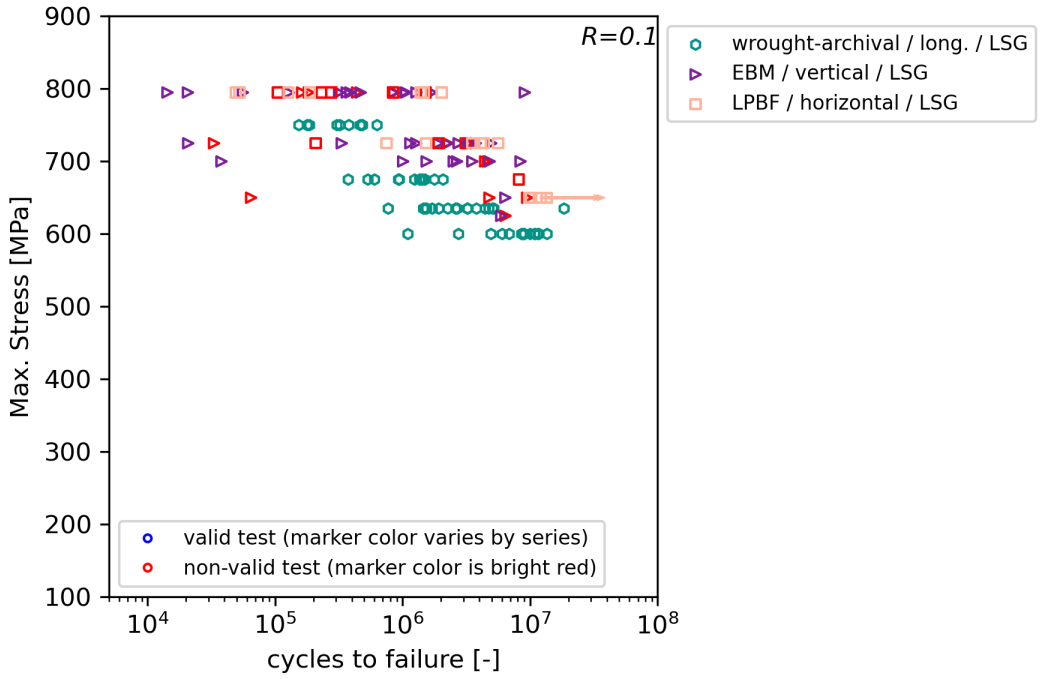

(b)

Fig. 3: Series are labeled according to the following schema: modality (LPBF, EBM, or wrought) / orientation relative to fabrication process (vertical or horizontal vs. a vertical build direction for AM; or longitudinal for plate forging); and surface condition (as-built or LSG). Data were divided into plots (a) and (b) for clarity.

Initiation features on fracture surfaces typical of machined LPBF specimens, as-built LPBF specimens, machined EBM specimens, and machined wrought specimens are shown in Fig 4. All specimens shown in Fig. 4 correspond to fatigue lifetimes of 2.8-4.1x10^5 cycles. In general, for specimens such as these which are tested under conditions causing failure after fewer than 1x10^6 load cycles fatigue cracks tend to be surface-initiated, while crack initiation in specimens that fail under conditions producing longer lives tends to be internal. Specimens with as-built surfaces are exceptions to this trend, as at all stresses they exhibit multiple competing surface cracks owing to the rough surface which provides many opportunities for crack initiation. To generalize, fatigue fracture initiation features are most often crystallographic in machined surface specimens fabricated by EBM (followed by HIP), and are usually due to round pores in machined surface specimens fabricated by LPBF (followed by combined SR and solutionizing). Wrought mill-annealed (MA) specimen fractures always bear crystallographic initiation features. LPBF specimens with machined and as-built surfaces also often have some features with crystallographic character immediately surrounding the initiation locations, but these have an appearance distinct from the wrought specimens due to their thermal history which produces a fully lamellar alpha structure. By contrast the wrought specimens are mill-annealed and have a duplex α+β microstructure with approximately 60 vol. % equiaxed primary alpha. These microstructural differences are expressed in the fracture morphologies at the initiation sites.

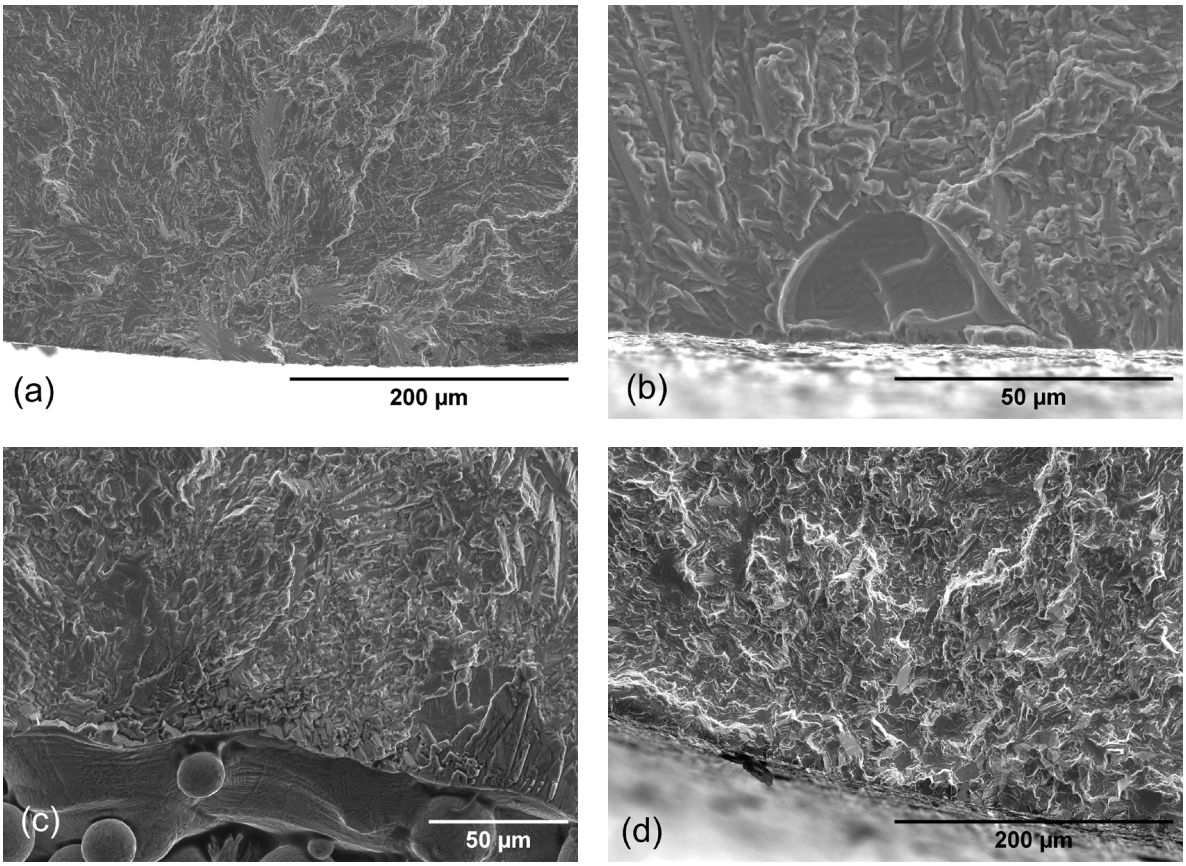

Fig 4: Fracture surface initiation sites from (a) machined surface EBM (HIP); (b) machined surface LPBF (stress-relieved); (c) as-built surface LPBF (stress-relieved); (d) machined surface wrought (mill-annealed) specimens.

The FCGR results for LPBF specimens at R = 0.1 are presented in Fig. 5 in terms of crack growth rate, *da/dN,* vs. stress intensity factor range, *ΔK*. Thirteen samples are plotted in total, from four different builds. In addition, the two FCGR laws used for calculating EIDS values, described below, are plotted

for reference. In the Paris regime, da/dN - ΔK data shows the expected linear trend in log-log space. A step-wise trend in the data was consistently noted in the lower Paris regime. As indicated by Fig. 5, FCGR behavior of the material was similar for the two orientations, Z-X and X-Z, considered in this study. Also, the results were consistent for specimens across multiple builds.

EIDS values were calculated by modeling the gage section as a rod in tension in which is embedded a semi-elliptical surface crack with semi-axes a (depth) and c (surface-connected half-length) with $c = a$, for which the Newman-Raju K solution is adopted [11]. In the model the crack advances according to a FCGR law described below, and using the experimental loading conditions. In this work several values for the maximum cycle stress, σ_{max}, were used, but the load ratio, R, was always 0.1.

Crack growth rates were modeled using a continuous three-part piecewise Paris-law fit (Fig. 5). A similar three-part Paris-law fit is used by Larsen et al. to represent fatigue crack growth behavior in Ti-6Al-4V [12]. To approximate small-crack behavior, crack growth rates in the lowest ΔK segment of the fit were extrapolated to arbitrarily small da/dN values. Although this approach omits long-crack threshold effects, it also ignores the faster crack growth rates typically observed at low ΔK during small crack growth [13,14]. Improved models accounting for elevated growth rates for short cracks will be incorporated in continuing work.

The FCGR fitting data for wrought specimens was drawn from previously-reported da/dN vs ΔK data [10]; the data for AM specimens was measured from experiments in the present work, except at the lowest ΔK values ($\leq$ 9.8 MPa$\sqrt{m}$ range), where data collection is still in progress. Fitting data for AM materials in that range were drawn from previously-published data for EBM Ti-6Al-4V [15], and joined to the higher ΔK-range data from the present work to construct a continuous three-part Paris-law fit. Fatigue tests that were either non-valid, resulted in run-out (>1x10^7 cycles without failure), or had internal crack initiation events, were excluded from the EIDS analysis. A log-probability plot of the resulting EIDS distributions for all specimens meeting these criteria is shown in Fig. 6. Counts of specimens that were tested, valid, and used in EIDS calculations (valid, non-runouts, and surface initiation), as well as 90th percentile and maximum EIDS values for each specimen class are reported in Table 4.

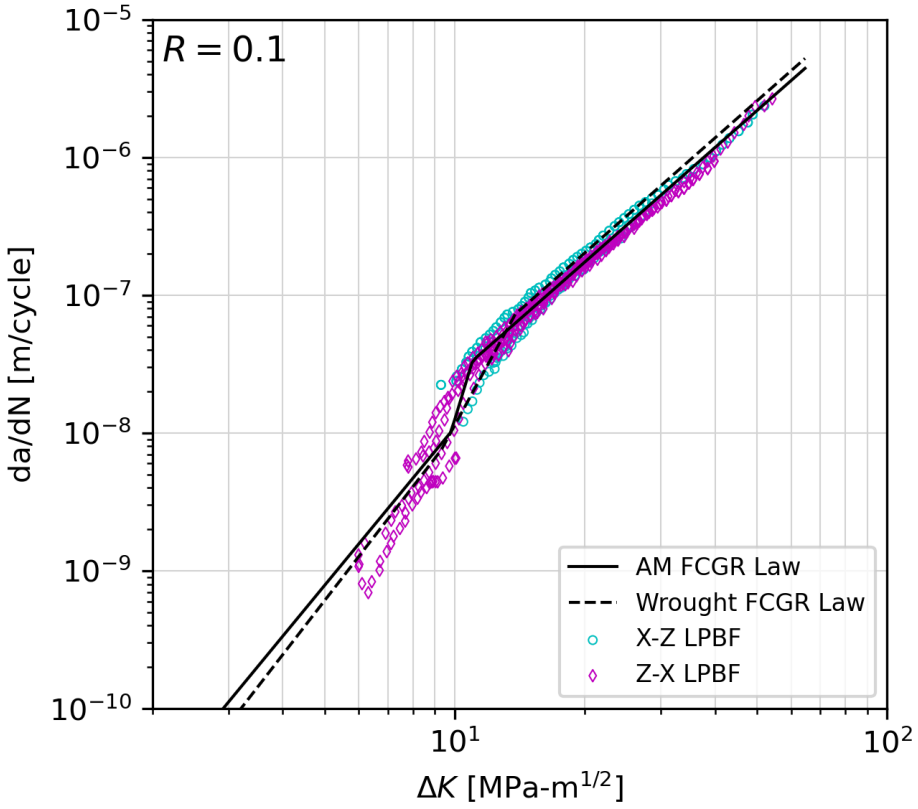

Fig 5: FCGR results in terms of *da/dN* vs. *ΔK* on LPBF Ti-6-4 at R = 0.1.

DISCUSSION

A core benefit of additive manufacturing is the ability to produce complex, net- or near-net shape parts that cannot be fabricated efficiently using conventional methods. To fully realize this benefit requires processes that minimize surface machining and post-processing, as such operations diminish the economic justification of AM fabrication. Further, in some instances critical surfaces may be inaccessible to effective surface improvement processes. For structural aerospace applications, it is therefore important to compare the DADT performance of machined wrought material (incumbent material capability); AM material with machined surfaces (inherent AM material capability); and AM material with as-built surfaces (recoverable AM material capability).

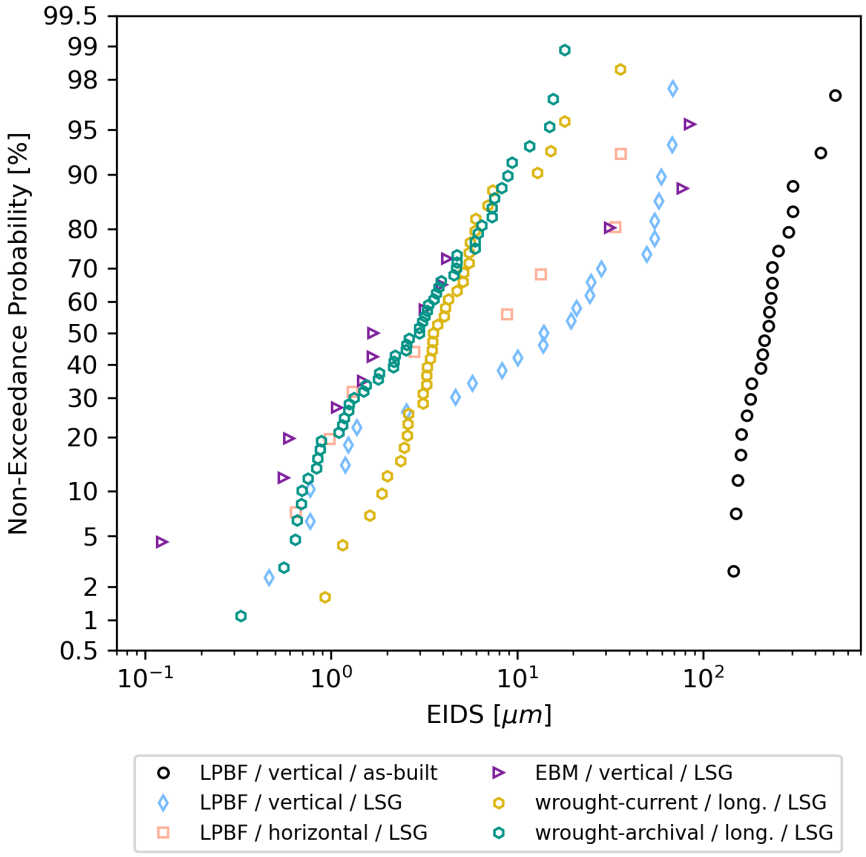

Fig. 6: Distributions of calculated EIDS values - runout tests, non-valid tests, and tests with internal crack initiation sites were excluded.

Fatigue results (Fig. 3) and EIDS distributions (Fig. 6 and Table 4) both make clear that the rough as-built surface (Fig. 2) significantly reduces the material quality for DADT performance, resulting in approximately an order of magnitude increase in maximum EIDS values from 36-83 µm in machined AM specimens to 512 µm in as-built LPBF specimens. All fractography conducted to date on as-built specimens suggests that fatigue cracks initiate from valleys in the rough surface. Analysis of longitudinal cross-sections of failed as-built bars (not shown here due to length constraints) reveals cracks emanating from many valleys adjacent to the fracture surface, lending supporting evidence that such features are the principal crack initiation sites. Upon completing the testing series and applying finalized crack growth rate models it will be possible to perform a statistical analysis of the EIDS distributions to determine the appropriate EIDS values for use in NC, DC, and FC DADT analyses as described in [2] (Table 1). The current incomplete dataset contains only 22 as-built LPBF EIDS results, yet the maximum calculated EIDS value (512 µm) is 39% of the minimum $1x10^{-7}$ probability of exceedance value used for Damage Tolerance analysis of FC parts (1300 µm). Therefore it is not unlikely that the final EIDS value for specimens with as-built surfaces will exceed that minimum value. It is also very likely that the final as-built EIDS value for Durability Analysis will exceed the minimum applicable EIDS value for NC and DC parts. In ongoing work to be presented elsewhere, a detailed statistical analysis of the roughness features in as-built gage section surfaces will be used to interpret the EIDS results, as well as to conduct probabilistic life analysis incorporating small-crack growth.

Table 4: Specimen counts and EIDS values for each specimen class

Specimen class	Total number of specimens	Number of valid, non-runout specimens	Number of specimens in EIDS plot[1]	$EIDS_{90}$ [μm]^2	$EIDS_{max}$ [μm]^3
LPBF / vertical / as-built	53	22	22	426	512
LPBF / vertical / LSG	57	40	25	68	69
LPBF / horizontal / LSG	22	15	8	36	36
EBM / vertical / LSG	48	35	12	83	83
wrought-current / long. / LSG	58	37	37	13	36
wrought-archival / long. / LSG	75	75	75	9	18

1. EIDS data are plotted for tests that were valid, not run-outs, and which exhibited surface initiation
2. Smallest value in the EIDS distribution having a probability of non-exceedance of at least 90%
3. Maximum value in the EIDS distribution for the number of samples in the EIDS plot

The two groups of wrought specimens (current and archival) had identical source material pedigree. The only difference between the two groups is that the machining and testing operations for the current specimens occurred with a 15-year delay relative to the archival specimens, and the σ_{max} values tested were not identical. The EIDS values for the current wrought specimen testing are similar to those of archival specimen testing, though shifted to somewhat larger values for the lower quantiles in the EIDS distributions (Fig. 6).

A substantial fraction of machined AM specimen fatigue test results could not be used in EIDS calculations (Table 4), primarily due either to the tests being run-outs, or to the fractures having been initiated at internal sites rather than surface sites. Efforts are currently underway to define analysis methods for including both runouts and internal initiation results in the EIDS analysis, significantly expanding the available data. A detailed comparison of EIDS distributions in machined AM specimens versus machined wrought specimens will be conducted in continuing work following these efforts, as well as continued fatigue testing. At this point, however, all classes of machined AM specimens have 90th percentile and maximum EIDS values (36-83 μm) that are similar to the 90th percentile (9-13 μm) and maximum (18-36 μm) EIDS values in wrought specimens, albeit slightly larger. These values are all significantly smaller than the minimum EIDS values required for DADT analyses (250-1300 μm, Table 1 [2]).

Fractography is being conducted on every failed fatigue specimen in this effort, and it is expected that the class, size, and distance of the initiating feature from the gage section surface will lend significant understanding to the fatigue testing and EIDS analysis results. In addition, full FCGR curves specific to all combinations of build orientation, crack-growth orientation, and AM modality; as well as a parallel study linking extensive computed tomography analysis of fatigue gage sections to serial-sectioning ground-truth data will help to better understand the populations of initiating features in each specimen class. This will contribute to the interpretation of part quality in the context of USAF DADT requirements for AM metals.

CONCLUSION

LPBF and EBM processes were used to fabricate round-bar fatigue and FCGR test specimens from Ti-6-4 with fully lamellar α+β microstructure. Plate forgings were used to fabricate round-bar Ti-6-4 fatigue specimens with duplex α+β microstructure (60% primary alpha). One series of LPBF specimens was fatigue tested with vertical as-built gage section surfaces, while all other samples were machined with LSG gage section surfaces. Fatigue and FCGR test results were used as inputs to an EIDS distribution analysis. The principal result is that the upper quantiles of EIDS values for as-built LPBF Ti-6-4 specimens were approximately an order of magnitude larger than those of machined samples in all other classes. This is due to the fact that the crack-initiation features in machined samples (round pores, alpha colonies, other crystallographic features) are less damaging than the deepest valleys that initiate cracking in as-built samples. There is additional nuance in the fatigue results and EIDS distributions for machined sample surfaces. A full analysis of those details in the context of DADT qualification of AM metals for the USAF will be given in future reporting of ongoing work.

ACKNOWLEDGEMENTS

We wish to acknowledge Luke Sheridan at the Air Force Research Laboratory for valuable conversations. Thad Kacsandy of UDRI and David Fink formerly of UDRI were instrumental in executing the LPBF builds; Christopher Ledford of Oak Ridge National Laboratory performed the EBM builds. Philip Blosser, Dale Osborne, Emily Meredith and James Coleman of UDRI conducted the mechanical property tests. Jared Shank of UES collected images of gage section surfaces and fatigue specimen fracture surfaces.

REFERENCES

[1] USAF, MIL-STD-1530D / Change 1, (2016).
[2] AFLCMC/EZ, Structures Bulletin EZ-SB-19-01, (2019).
[3] R. Jones, R.K.S. Raman, A.P. Iliopoulos, J.G. Michopoulos, N. Phan, D. Peng, Additively manufactured Ti-6Al-4V replacement parts for military aircraft, Int. J. Fatigue. 124 (2019) 227–235. https://doi.org/10.1016/j.ijfatigue.2019.02.041.
[4] A.P. Iliopoulos, R. Jones, J.G. Michopoulos, N. Phan, C. Rans, Further Studies into Crack Growth in Additively Manufactured Materials, Materials. 13 (2020) 2223. https://doi.org/10.3390/ma13102223.
[5] ASTM F2924 − 14: Specification for Additive Manufacturing Titanium-6 Aluminum-4 Vanadium with Powder Bed Fusion, ASTM International, 2021. https://doi.org/10.1520/F2924-14R21.
[6] ASTM E8/E8M − 21: Test Methods for Tension Testing of Metallic Materials, ASTM International, 2021. https://doi.org/10.1520/E0008_E0008M-21.
[7] ASTM E466 − 15: Practice for Conducting Force Controlled Constant Amplitude Axial Fatigue Tests of Metallic Materials, ASTM International, 2015. https://doi.org/10.1520/E0466-15.
[8] ASTM E647 − 15: Standard Test Method for Measurement of Fatigue Crack Growth Rates, ASTM International, 2015.
[9] J. Larsen, J. Jira, K. Ravichandran, Measurement of Small Cracks by Photomicroscopy: Experiments and Analysis, in: J. Larsen, J. Allison (Eds.), Small-Crack Test Methods, ASTM International, West Conshohocken, PA, USA, 1992: pp. 57-57–24. https://doi.org/10.1520/STP15064S.
[10] J.H. Gallagher, R.H. vanStone, R.E. deLaneuville, R.S. Gravett, D.C. Bellows, D.C. Slavik, S.J. Hudak, T.J. Dunyak, Berens, Improved High-Cycle Fatigue Life Prediction, Air Force Research Laboratory, Wright-Patterson AFB, OH, USA, AFRL-ML-WP-TR-2001-4159, 2001.
[11] I.S. Raju, J.C. Newman, Jr., Stress-intensity factors for circumferential surface cracks in pipes

and rods under tension and bending loads, NASA-TM-87594, 1985.

[12] J.M. Larsen, A.H. Rosenberger, A.L. Pilchak, N.E. Young, P.A. Sherer, P.J. Golden, R. John, Effects of cold-dwell fatigue on the growth of long cracks in alpha+beta Ti-6Al-4V, in: Proceedings of the 15th World Titanium Conference, Ti-2023, Edinburgh, UK, 2023.

[13] M.J. Caton, R. John, W.J. Porter, M.E. Burba, Stress ratio effects on small fatigue crack growth in Ti–6Al–4V, Int. J. Fatigue. 38 (2012) 36–45. https://doi.org/10.1016/j.ijfatigue.2011.11.004.

[14] P.J. Golden, A. Whitney-Rawls, S.K. Jha, W.J. Porter III, D. Buchanan, K. Prasad, V. Chandravanshi, V. Kumar, R. John, Probabilistic prediction of minimum fatigue life behaviour in α + β titanium alloys, Fatigue Fract. Eng. Mater. Struct. 42 (2019) 674–685. https://doi.org/10.1111/ffe.12942.

[15] S. Draper, B. Lerch, R. Rogers, R. Martin, I. Locci, A. Garg, J. Telesman, Materials Characterization of Electron Beam Melted Ti-6Al-4V, Glenn Research Center, Cleveland, OH, NASA/TM-2016-219136, 2016. https://ntrs.nasa.gov/citations/20160011332.